Catalysis Science & Technology

ROYAL SOCIETY OF CHEMISTRY

PAPER

View Article Online
View Journal | View Issue

Cite this: *Catal. Sci. Technol.*, 2023, **13**, 862

Alumina binder effects on the hydrothermal stability of shaped zeolite-based catalyst bodies

Nikolaos Nikolopoulos, Abhijit Wickramasinghe, Gareth T. Whiting* and Bert M. Weckhuysen*

The development of shaped zeolite-based catalyst bodies with high performance for the production of fuels and chemicals requires the addition of binder materials. Thus, alumina binder effects and their impact on the hydrothermal stability are crucial for shaped catalyst bodies and their catalytic performance in the methanol-to-hydrocarbon (MTH) reaction. Here, a side-by-side comparison of zeolite powder and zeolite–alumina catalyst extrudates is made to elucidate the effect of the extrusion process and/or the hydrothermal treatments in combination with the binder effects. Characterization of the acidic properties was carried out with Fourier-transform infrared (FT-IR) spectroscopy to understand the role of the binder material. It was found that the alumina binder increases the Lewis acidity, while it protects the zeolite material from dealumination during the hydrothermal treatments. Testing of the samples, before and after steaming, showed that the extrusion and steaming lead to a more stable and selective catalyst material, while altering the physicochemical properties of the alumina binder plays a crucial role in achieving the optimal ethylene-to-propylene ratio. *Operando* UV-vis diffuse reflectance spectroscopy (DRS) revealed the higher formation of conjugated polyaromatic species for the technical catalyst bodies. This study illustrates the impact of the extrusion process and the binder material in combination with the hydrothermal treatments and the major effect of the binder properties on the physicochemical properties and the product distribution.

Received 3rd November 2022,
Accepted 14th December 2022

DOI: 10.1039/d2cy01894b

rsc.li/catalysis

Introduction

The large-scale production of (petro)chemicals requires the development of industrial catalysts in the form of technical bodies, which can achieve high catalytic performance.[1–4] However, the route from a lab-scale powder catalyst to the scale-up of a catalyst body is usually challenging. A few parameters need to be taken into account as they can profoundly affect the final properties of the catalyst material, such as the formulation and the shaping parameters. Only a limited number of studies in the open literature focus on a deeper understanding of these binder effects.[1,5–9] A better understanding of these effects is essential in more complex and multi-component zeolite-based shaped catalyst bodies as they could alter the physicochemical properties due to zeolite–binder interactions.[2–4,10,11]

Due to the increase of propylene and ethylene demand, the methanol-to-hydrocarbon (MTH) process is an important chemical conversion process for producing lower olefins (C_2–C_4). While most studies in the literature have focused on zeolite powder samples,[12–14] only a few studies have underlined the importance of binder effects in zeolite-based shaped catalyst materials and their influence on the physicochemical properties and catalytic activity.[9,15–18] Over the past decades, various zeolite framework structures, with the most promising results coming from MFI (*i.e.*, ZSM-5) and CHA (*i.e.*, SAPO-34 and SSZ-13) catalysts, have been investigated to unlock the interplay between physicochemical properties (acidity and porosity), reaction conditions, and catalytic performance.[12,19,20]

Several modifications in zeolite powder catalysts have been studied, as acidity and porosity have a key role in catalytic activity to achieve higher selectivity towards light olefins. Post-synthesis modification, such as metal incorporation (*e.g.*, Mg and Ca), is, among others, a strategy to enhance light olefin yields.[21–28] It has been proved that metal-modified zeolites exhibited higher selectivity towards ethylene and propylene, while the lifetime of the catalyst materials was improved. Altering the Si/Al ratio and, consequently, the strength and the density of Brønsted acid sites (BASs) has been beneficial for the catalyst performance in the MTH process. Dealumination and/or desilication *via* post-synthesis modification of zeolites can achieve the aforementioned

Inorganic Chemistry and Catalysis, Debye Institute for Nanomaterial Science, Utrecht University, Universiteitsweg 99, 3584 CG Utrecht, The Netherlands. E-mail: gtwhiting1@gmail.com, B.M.Weckhuysen@uu.nl

changes in the properties of the zeolite catalyst and improve the lifetime of the catalyst material and the selectivity towards light olefins.[16,29–31]

In the quest to move from catalyst powders to technical catalyst bodies, Pérez-Ramírez and co-workers investigated the binder effects (*i.e.*, silica, alumina, and clays used as binder materials) on the physicochemical properties of zeolite ZSM-5-based catalyst extrudates. It was found that silica and/or alumina promoted the formation of larger hydrocarbons in the MTH reaction, while when attapulgite was used as a binder material both the lifetime of the catalyst and the selectivity to propylene and butylenes increased.[9] Lee *et al.* studied in detail the effect of three different binder materials (*i.e.*, silica, alumina, and aluminum phosphate) on the acidity, texture, and mechanical strength and the catalytic activity in the methanol-to-olefin (MTO) reaction of zeolite HZSM-5-based technical bodies. Altering among silica, alumina, and/or aluminum phosphate binders affected the acidity of the sample as the Al_2O_3 binder had a slight increase in the number of strong acid sites, while using silica and aluminum phosphate as binder materials resulted in a decrease in the number of strong acid sites. Consequently, low content silica- or alumina-bound extrudates had a similar selectivity towards light olefins and aluminum phosphate-bound extrudates exhibited enhanced propylene selectivity. In the same study, binary systems were further investigated to find the best balance between properties and catalytic activity. Thus, it was shown that silica/alumina combined with aluminum phosphate exhibited similar propylene selectivity and higher mechanical strength compared to when only aluminum phosphate was used as a binder.[32]

Zhang *et al.* investigated the effect of hydrothermal treatment on zeolite powders and alumina-bound extrudates on the acidity of the samples and their catalytic performance in the methanol-to-propylene (MTP) reaction. It was shown that these catalyst extrudates exhibited higher Lewis acidity due to the presence of an alumina binder, which was preserved even after steaming. Regarding the MTP performance of the catalysts, the extruded zeolite sample showed a different product distribution and a slightly increased lifetime, which is attributed to the alumina binder. The hydrothermal treatment of the catalyst extrudates and powders increased the selectivity towards propylene and led to a significant increase in the lifetime during the MTP process as steamed catalyst extrudates exhibited 89 h, while steamed zeolite powder had a lifetime of only 57 h. The latter was attributed to fine-tuned acid sites due to alumina addition and steaming.[16]

Thus, it would be of great importance to further understand and control binder effects. Here, we have investigated the impact of the alumina binder material and hydrothermal treatment on the physicochemical properties and the MTH performance using a combination of *ex situ*, *in situ*, and *operando* advanced characterization techniques. Zeolite ZSM-5 powder and alumina-bound extrudate samples were hydrothermally treated for different times at 500 °C to understand the changes induced by steaming in the zeolite framework structure, the acidity, and the catalytic performance. Fourier-transform infrared (FT-IR) spectroscopy was employed to study the structural changes due to extrusion and steaming. FT-IR spectroscopy in combination with pyridine as a probe molecule was used to investigate the changes in the Brønsted and Lewis acidity. It was proven that the extrudate sample has a higher amount of Lewis acidity and resistance in dealumination. Extrusion of zeolites in combination with steaming resulted in a more stable catalyst with a propylene yield, while it was shown that the properties of the alumina binder could alter the ethylene-to-propylene ratio. A mechanistic investigation under realistic conditions using *operando* UV-vis diffuse reflectance spectroscopy (DRS) was performed in order to understand the effect of hydrothermal treatment and the binder effects on the MTH reaction. This study proves the necessity for a deeper understanding of multi-component shaped catalyst bodies and the impact of the binder properties and the hydrothermal treatments on their physicochemical properties and catalytic performance.

Results and discussion

Powders *versus* extrudates: effect of the binder

The zeolite ZSM-5 powder samples were compared with the alumina-bound zeolite-based catalyst extrudates before and after hydrothermal treatment to unravel the effect of the extrusion process and the impact of steaming on the physicochemical properties and the catalytic performance of the zeolite-based materials.

The zeolite ZSM-5 powder samples and the zeolite/alumina extrudates were hydrothermally treated at 500 °C for 7 h. Fig. 1a shows the XRD patterns of the parent and the steamed zeolite ZSM-5 powder and extrudate samples. In general, XRD shows the characteristic peaks of an MFI structure for all the samples under study. Comparing the XRD patterns for the zeolite powder (black) and zeolite-based extrudate (red) samples, no significant difference can be noticed, indicating that the extrusion process did not affect the zeolite structure. After 7 h of severe steaming of the zeolite powder (grey) sample, there is a decrease in the peak intensity and a broadening of the XRD peaks, as shown clearly in the zoomed-in graph in Fig. 1a, which implies the partial damage of the zeolite framework. The latter can be attributed to the hydrolysis of aluminum atoms from the zeolite framework structure. After a close inspection of the peak at 2theta equal to ~28.3° (yellow highlighted area), it is observed that splitting of the peak occurs upon steaming due to the presence of monoclinic symmetry.[33,34] The same observations also stand for the steamed catalyst extrudate sample.

From the NH_3-TPD analysis data, which are shown in Fig. 1b, the strength and the total amount of acid sites are determined. The parent zeolite ZSM-5 powder sample (black) shows two major peaks at ~250 °C and at ~445 °C and a

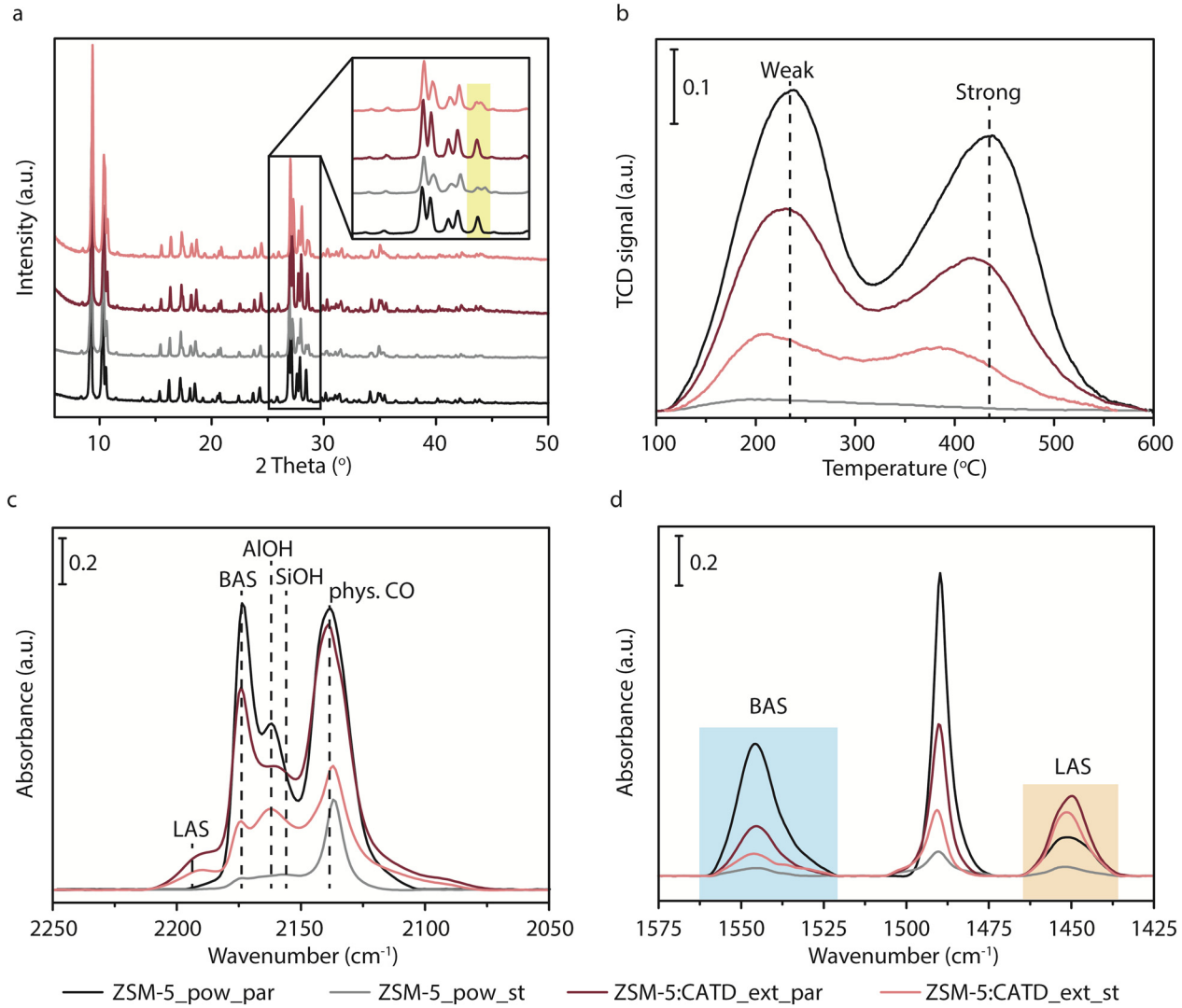

Fig. 1 Structural and acidic properties before and after steaming. a) X-ray diffraction (XRD) pattern, b) ammonia temperature-programmed desorption (NH_3-TPD) analysis, c) CO adsorption followed by Fourier-transform infrared (CO-FT-IR) spectroscopy data measured at 10 mbar and −188 °C, and d) pyridine adsorption followed by Fourier-transform infrared (Py-FT-IR) spectroscopy data measured at 150 °C of the parent and steamed zeolite ZSM-5 in their powder and extrudate form (denoted as ZSM-5_pow_par, ZSM-5_pow_ext, ZSM-5_ext_par and ZSM-5_ext_st, accordingly). The latter spectra were normalized. Inset in (a) show the 2θ 25–30° region.

total acidity of 1.01 mmol g^{-1}. The peak at ~250 °C represents weak acid sites, while the peak at ~445 °C is assigned to strong acid sites.[35–37] When zooming in on the parent extrudate sample (red), the overall acidity is reduced to 0.66 mmol g^{-1} compared to 1.01 mmol g^{-1} of the parent powder sample. This was expected as the extrudate sample contains 50% zeolite and 50% alumina. Additionally, this reduction in acidity could be justified from partial coverage of the zeolite surface by the alumina binder and the migration of Al species resulting in pore blockage.[1,5,18] Furthermore, a slight shift of the two peaks at lower temperatures indicates the weakening of the acid sites due to the effect of the extrusion process. Severe steaming of the zeolite powder sample (grey) resulted in almost complete elimination of the acid sites of the zeolite (0.08 mmol g^{-1}). Interestingly, the steamed extrudate sample (pink) preserved relatively higher acidity than the sample after the hydrothermal treatments. The latter confirms the significant impact of the alumina binder on hydrothermal stability as it proves that the alumina binder prevented the zeolite from its complete loss of acidity.

Fig. 1c shows the CO-FT-IR spectroscopy experiments, revealing the nature of the different –OH groups present for the samples under study. The samples, after CO adsorption, present several peaks located at 2191, 2175, 2162, 2158, and 2138 cm^{-1}, which correspond to Lewis acid sites (LASs), Brønsted acid sites (BASs), extra-framework Al–OH (EFAlOH), silanol groups, and physisorbed CO, respectively.[26,38] The parent zeolite powder sample (ZSM-5_pow_par, black) shows LASs, BASs, EFAlOH, and silanol groups. Regarding the extrudate parent sample (denoted as ZSM-5_ext_par, red), it can be noted that it contains the same –OH groups, but in

different relative intensities, while it exhibited lower amounts of BASs and LASs. This can be attributed to the alumina binder as the aluminum species can act as LASs or damage the zeolite framework upon extrusion. After steaming the zeolite powder (ZSM-5_pow_st, grey), low intensity FT-IR peaks for all types of –OH groups can be observed, confirming the results from the NH_3-TPD analysis.

The Py-FT-IR spectroscopy experiments are shown in Fig. 1d, in which the peak at 1445 cm^{-1} can be assigned to LASs and 1545 cm^{-1} to BASs.[39–41] Prior to steaming, the acidity of the zeolite powder sample is governed by BASs, while the catalyst extrudate appears with a higher amount of LASs. As aforementioned, LASs in the catalyst extrudates can be attributed to the presence of the alumina binder. Furthermore, after steaming, the powder sample showed a significant decrease in the number of BASs and LASs while the catalyst extrudate sample showed a high number of LASs and a decreased number of BASs. All in all, it is clear from the results obtained from Py-FT-IR, CO-FT-IR, and NH_3-TPD that the presence of the alumina binder is crucial for the development of the acidic properties of the zeolite material as it not only alters the BAS and LAS ratio, but also increases the hydrothermal stability of the zeolite as it protects the zeolite framework from dealumination.

The zeolite powder samples and the alumina-bound zeolite-based extrudate samples are hydrothermally treated for different times (*i.e.*, 15, 30, 60, 120, 210, and 420 min) while FT-IR spectroscopy is used to probe the changes in the –OH stretching region. As shown in Fig. 2a, the parent zeolite powder sample shows four peaks centered at 3742, 3724, 3663, and 3610 cm^{-1} which can be attributed to the presence of SiOH groups in external and mesopore surfaces, SiOH in defects, EFAlOH, and BASs.[42,43] It is observed that there is a decrease in the number of BASs and, consequently, an increase in extra-framework Al species (EFAL) due to hydrolysis of Al upon steaming. However, the zeolite-based catalyst extrudates, shown in Fig. 2b, seem to differ from the powder sample before and after steaming. Comparison of the parent samples, powder and extrudates, revealed that the extrusion process induces changes in the –OH groups as there is an apparent relative decrease in the number of BASs and a relative increase in the number of SiOH defects. Furthermore, upon extrusion, extra peaks are present at 3773 and 3680 cm^{-1}, which can be attributed to extra-framework single tetrahedral Al sites and the bridging –OH group coordinated to two Al cation sites (Al–OH–Al), accordingly, due to the presence of the alumina binder.[44,45] The alumina-bound zeolite-based extrudate samples showed resistance in BAS loss and a relative increase in the number of Al–OH–Al and SiOH groups in defect positions with increasing steaming time. The relative increase of Al–OH–Al can be attributed to the hydrolysis of the alumina binder, while the increase of SiOH can explain the high amount of LASs present after steaming, as previously explained.

Fig. 3 shows the results of the Py-FT-IR spectroscopy measurements of each sample, powder and extrudates, prior to and after each steaming time to elucidate the changes in the acid sites induced by the steaming process. The parent zeolite powder sample exhibits a significant loss in the number of BASs, as shown in Fig. 3a and c, while the extrudate sample shows to be more robust towards a loss of BASs. A higher amount of BASs is noted in the powder sample compared to extrudates, even after normalization based on the zeolite content, which can be attributed to

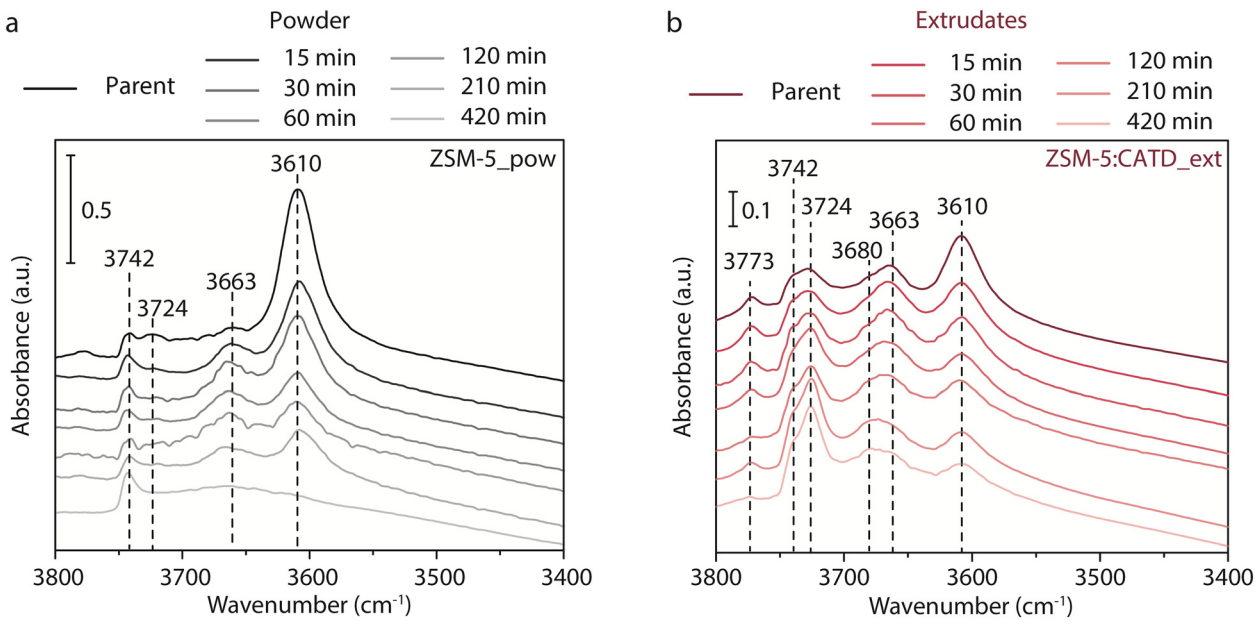

Fig. 2 Probing the changes in the –OH groups upon steaming. Fourier-transform infrared (FT-IR) spectra taken under vacuum after drying the samples at 550 °C for 2 h for the parent and steamed for 15, 30, 60, 120, 210, and 420 min. a) Zeolite ZSM-5 powder (denoted as ZSM-5_pow, black) and b) zeolite-based catalyst extrudates (denoted as ZSM-5:CATD, red).

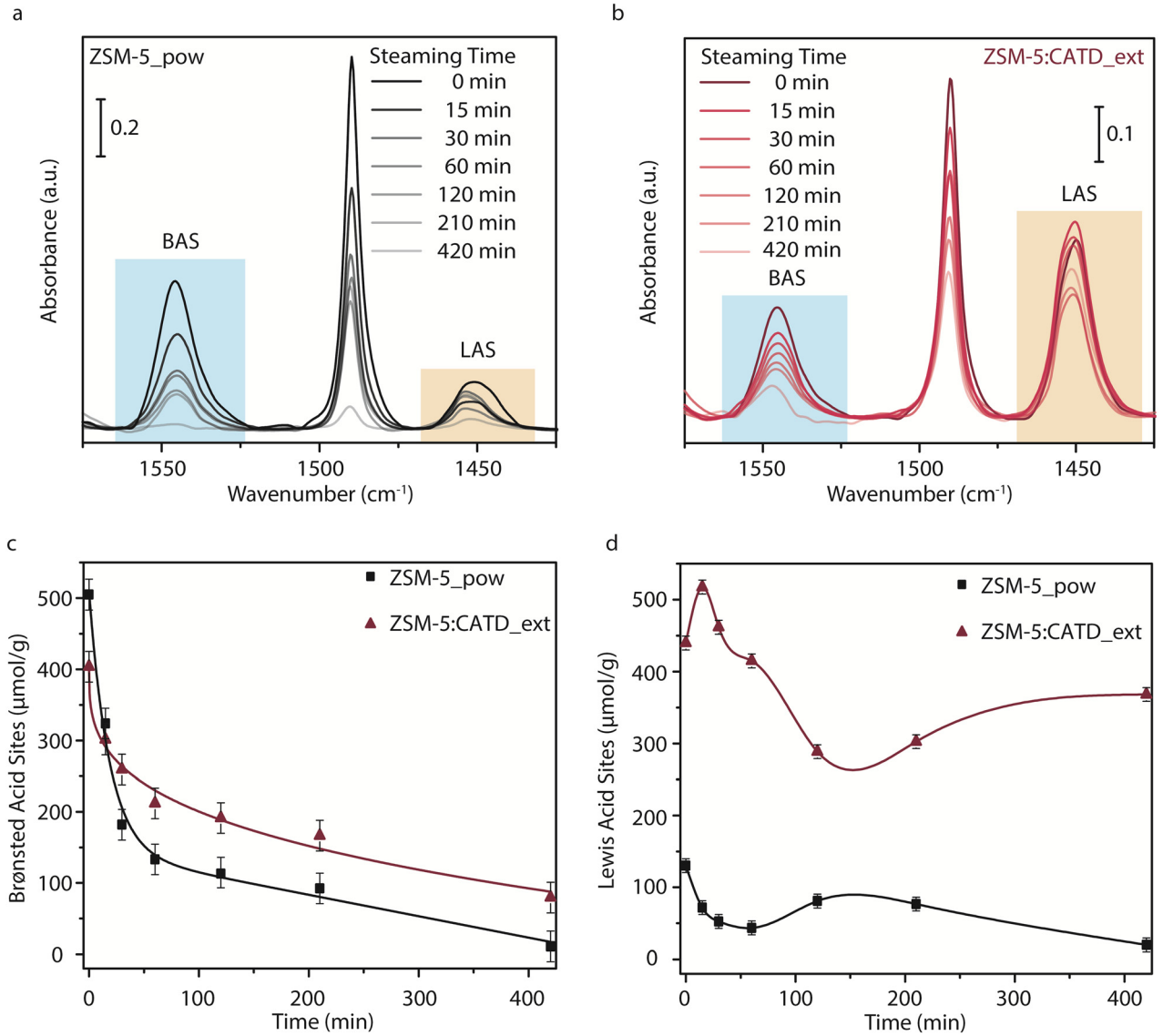

Fig. 3 Changes in Brønsted and Lewis acidity induced by steaming. Pyridine adsorption followed by Fourier-transform infrared (Py-FT-IR) spectroscopy measured at 150 °C of a) zeolite ZSM-5 powder (denoted as ZSM-5_pow, black) and b) zeolite-based catalyst extrudates (denoted as ZSM-5:CATD, red). c) Brønsted acid sites (BASs) and d) Lewis acid sites (LASs) *versus* steaming time of zeolite ZSM-5 powder (denoted as ZSM-5_pow, black square) and zeolite-based extrudates (denoted as ZSM-5:CATD, red triangle) (only the BAS curve was normalized based on the zeolite content for the extrudate sample).

dealumination during the extrusion process. Overall, the extrudate sample seems to be more stable under hydrothermal treatments as it maintains a higher number of BASs than the zeolite powder sample. Furthermore, the trend in the amount of Lewis acidity, as shown in Fig. 3d, for both types of samples seems to differ. The number of LASs in the zeolite powder sample starts decreasing upon applying short steaming times, and then there is an increase, while it shows a relatively low amount of LASs after 7 h of steaming. In contrast, the extrudate sample shows an increase in the number of LASs for short steaming time, and it preserves high levels of LASs even after 7 h of steaming.

Firstly, the surrounding binder material may protect the zeolite from acidity loss. Specifically, the alumina binder can also react with H_2O, explaining the sharp increase in the number of LASs during short steaming times, while the powder sample shows a decrease in the number of LASs. Furthermore, there is no mechanism proving that Al species could stabilize the acidity of zeolites without neutralizing the BASs.[46] Of course, it would be possible that the migration phenomena of Al species from the binder material to the zeolite framework can take place. However, there is no experimental evidence presented in this study that proves that such phenomena indeed occur. Last but not least, there is another theory in order to decode the differences in the changes of BASs which involves EFAL and BASs in close proximity. Coordination of $Al(OH)_3$ species (acting as LASs) to the nearest BAS oxygen atom can result in a partial electron

transfer to $Al(OH)_3$ species from –OH framework bonds. The latter phenomenon can decrease the strength of the OH bond and as a result can increase the strength of the acid sites.[47] However, the latter could not be justified in the systems under study as there was no shift in the BAS peak upon steaming, as shown in Fig. 3a and b.

Fig. 4 shows the catalytic conversion and the yields towards ethylene and propylene formed during the MTH reaction for the powder and the extrudate samples before and after steaming. The catalytic tests were performed at a weight hourly space velocity (WHSV) of 8 h^{-1} and 350 °C for 900 min time-on-stream (TOS). The parent zeolite powder sample shows high methanol conversion close to 100%, which decreases around ~300 min due to the high amount of BASs, while the extrudate sample shows a lower, but more stable conversion (~71%). The latter can be attributed to the decrease of the total acidity due to the partial dealumination of the zeolite material during extrusion and the pore blockage of the zeolite pores from the alumina binder as well as the lower zeolite content. After steaming, the powder sample still shows a high stable conversion (~85%), while the extrudate sample exhibits a lower stable conversion (~56%). Among the samples, the parent zeolite powder sample shows a higher yield towards ethylene and propylene. The extrudate sample showed a high enough yield towards light olefins, especially taking into account the decrease in acidity due to the lower zeolite content for the extrudate sample along with the pore blockage. After a treatment for 7 h at 500 °C, the steamed zeolite powder shows a yield towards light olefins close to zero, and methanol is only converted into dimethyl ether (results are not presented here for brevity). This could be explained by total dealumination of the zeolite material, resulting in a low amount of the weak acid sites present in the sample after steaming. However, even though treated under the same conditions as the powder samples, the catalyst extrudate sample exhibits a slightly lower ethylene yield and a higher propylene yield. These findings are in line with the literature, as Brønsted acidity is crucial for propylene selectivity. It is shown that decreasing the BAS concentration could enhance the selectivity towards propylene.[28] Here, it can be noted that the number of BASs decreases and the propylene yield increases upon steaming, while the ethylene yield decreases. To further evaluate the catalytic behavior of the samples and the effects of the extrusion process and the hydrothermal treatments, *operando* UV-vis diffuse reflectance spectroscopy (DRS) was performed, which is summarized in Fig. 5. UV-vis DRS can differentiate between hydrocarbon pool (HP) species and deactivating carbon species (*i.e.*, internal and external coke species). The samples show absorption bands at ~285 nm, ~335 nm, ~380 nm, ~418 nm, ~420 nm, and >500 nm, which can be attributed to neutral benzenes/polyalkyl-substituted cyclopentadienium ions with four or five alkyl groups, dienyl carbocations, highly methylated arenium ions, naphthalene and/or anthracene and methylated polyarenium ions/highly conjugated polyenes, respectively.[28,48–54]

The parent powder sample (ZSM-5_pow_parent) shows fast formation of neutral benzenes (~285 nm) as well as further formation of internal coke species, such as naphthalene and/or anthracene (~418 nm), which is attributed to the high amount of BASs in the sample. However, upon extrusion, a relatively less formation of neutral benzenes and naphthalene and/or anthracene is noted, while at the same time highly methylated arenium ions are observed. The decrease of the number of BASs can explain this phenomenon due to the extrusion process and the induced defects in the zeolite framework, as previously discussed. Further comparison of the parent powder and extrudate samples revealed the relatively higher formation of external coke species (>560 nm) for the extrudate sample, as shown in Fig. 5a and c. However, such observations may be in contrast with the fact that the extrudate samples contain more LASs and recent studies proving that LASs can inhibit reactions involving aromatic moieties.[26,28] The latter disagreement could be explained by the nature and the pore architecture of the two types of samples. More specifically, when zeolite powder catalyst materials are used, methanol has to diffuse in the zeolite pores and products has to diffuse out. The same

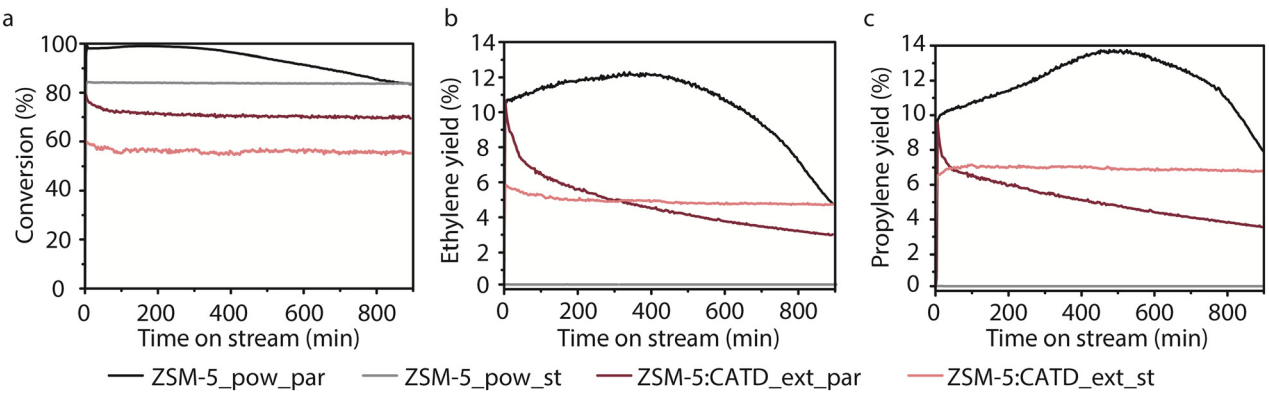

Fig. 4 Catalytic behavior in the methanol-to-hydrocarbon (MTH) reaction. Catalytic activity and selectivity of ZSM-5_pow_par (black), ZSM-5_pow_ext (grey), ZSM-5:CATD_ext_par (red) and ZSM-5:CATD_ext_st (pink) samples *versus* time-on-stream (TOS) for the MTH reaction performed at 350 °C with a weight hourly space velocity (WHSV) of 8 h^{-1}. a) Methanol conversion, b) ethylene yield, and c) propylene yield.

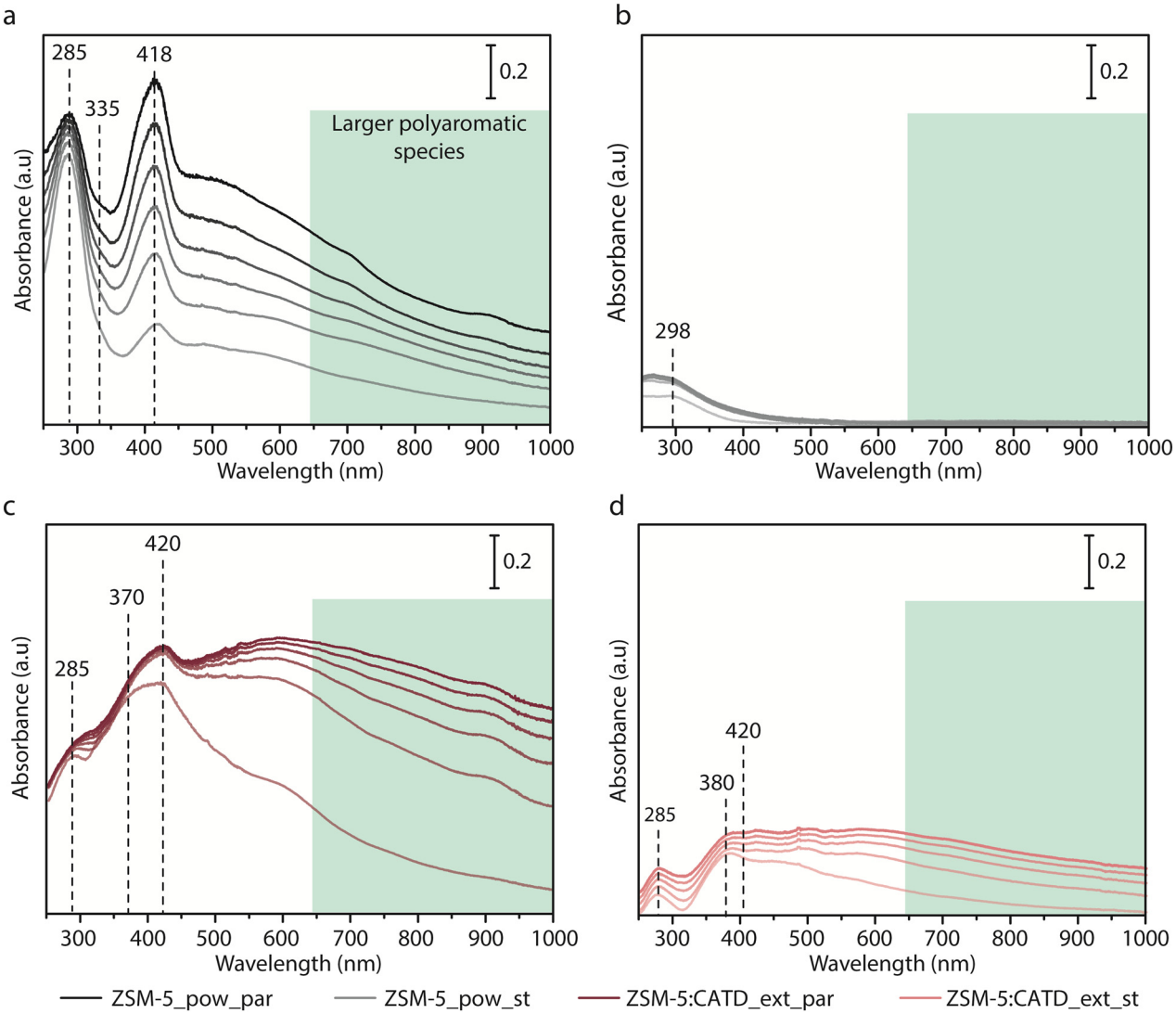

Fig. 5 Intermediate and coke species formation using *operando* UV-vis Diffuse Reflectance Spectroscopy. *Operando* ultraviolet-visible (UV-vis) diffuse reflectance spectroscopy (DRS) data for a) ZSM-5_pow_par (black), b) ZSM-5_pow_ext (grey), c) ZSM-5:CATD_ext_par (red), and d) ZSM-5:CATD_ext_st (pink).

approach has to be considered for the extrudate catalyst materials. However, the zeolite crystal is ~2 μm in size while the extrudate catalyst materials have a diameter of ~2 mm. Thus, it is inevitable to avoid successive and secondary reactions which will cause the formation of such polyaromatic species in the extrudate catalyst samples. This is also proved by a recent study of our group which has shown that larger aromatic species are formed, but they fall into secondary reactions where these molecules can oligomerize to produce even larger polyaromatic species that could cause the deactivation of the catalyst material as they could not diffuse out of the extrudate.[15] Using a micro-spectroscopic approach, the formation of a non-fluorescent zone (ring) was observed after 75 min time on stream, which could be attributed to the formation of larger polyaromatic molecules, while the core of the shaped catalyst bodies showed an orange/yellow (green and red) color due to the presence of a mixture of smaller and larger (poly)aromatic compounds. The aforementioned observations are in line with the *operando* UV-vis DRS measurements as the extrudate samples appeared to have a relatively higher formation of polyaromatic species.

Upon steaming, the zeolite powder sample shows hardly any formation of intermediate or coke species, which corresponds with the catalytic activity data, as we have explained above. In contrast, the steamed extrudate sample shows relatively lower formation of intermediate HP species as well as coke species while their nature is akin to those formed before steaming. It can be observed that even after steaming the extrudate sample shows the formation of larger polyaromatic species underlying the significant effect of the pore architecture and transport boundary in the deactivation of the shaped catalyst bodies during the MTH reaction.

Effect of the binder precursor materials on the properties and activity of shaped catalyst bodies

The results mentioned above proved the importance of the intimacy between the zeolite and binder, as well as the resulting changes in the physicochemical properties and the catalytic activity of the shaped catalyst bodies. However, the binder properties are often overlooked and, thus, we aimed to investigate the effect of the alumina–binder properties in this study. Two different boehmite (*i.e.*, alumina hydrates) binder precursor materials were chosen based on their physicochemical properties. CATAPAL D (denoted as CATD) exhibits a specific surface area (SSA) of 220 m^2 g^{-1}, and the crystallite size is 7 nm, while PURAL TH100 (denoted as TH100) exhibits 150 m^2 g^{-1} and the crystallite size is 14 nm. Therefore, the effect of the surface area and the crystallite size of the alumina binder on the subsequent properties and the catalytic performance before and after steaming is investigated. The set of samples using CATAPAL D as a binder precursor material has been used in the previous section to describe the effect of the alumina binder, and it will now further be compared to the set of samples using PURAL TH100.

As shown in Fig. 6a, the XRD patterns show characteristic peaks of an MFI structure for all the materials under study. It seems that the properties of the binder material do not have an impact on the zeolite framework structure upon extrusion. After steaming of the samples, in both cases, a decrease in the peak intensity can be noted, and splitting of the XRD peak at ~28.3° due to the removal of Al species from the zeolite framework during the steaming treatments was observed. Fig. 6b shows the –OH region of the FT-IR spectra of all four samples before and after 7 h of hydrothermal treatments. No significant differences present in the samples are noticed regarding the –OH group. All in all, the changes in specific surface area (SSA) and crystallite size of the alumina binder material did not affect the structure of the zeolite domains or the overall structure of the shaped catalyst bodies.

Fig. 7a shows the BET surface area for all the samples measured before and after steaming. The obtained results regarding the samples prior to steaming show a small effect of the binder properties on the final BET surface area of the catalyst extrudates as the sample containing CATAPAL D has 315 m^2 g^{-1} while the sample with TH 100 has 295 m^2 g^{-1}. After steaming, it seems that the difference in the BET surface area is preserved as ZSM-5:CATD_ext_st and ZSM-5:TH100_ext_st have 251 and 233 m^2 g^{-1}, accordingly.

Moving to the acidic properties of the materials, NH_3-TPD (Fig. 7b) shows a clear difference in the acidity of the two samples. This can be only attributed to the different binders as the zeolite content in each sample is kept the same. Two contributing factors can explain this phenomenon. Firstly, it could be argued that the two different binder (precursor) materials contribute to the genesis of different amounts of acid sites in the total acidity make-up of the shaped catalyst bodies. Secondly, the increased acidity of the sample where CATAPAL D was used as a binder material could be explained by the increased BET surface area and, thus, by an enhanced diffusion and a decreased pore blockage. The Py-FT-IR spectroscopy experiments, shown in Fig. 7c, revealed the same trend as the NH_3-TPD experiments as the sample made using PURAL TH100 as a binder precursor material has a lower number of BASs and LASs compared to the sample made using CATAPAL D as a binder precursor material. The differences noticed with Py-FT-IR spectroscopy are smaller compared to NH_3-TPD due to the nature of the analytical techniques as pyridine cannot probe the acid sites contained

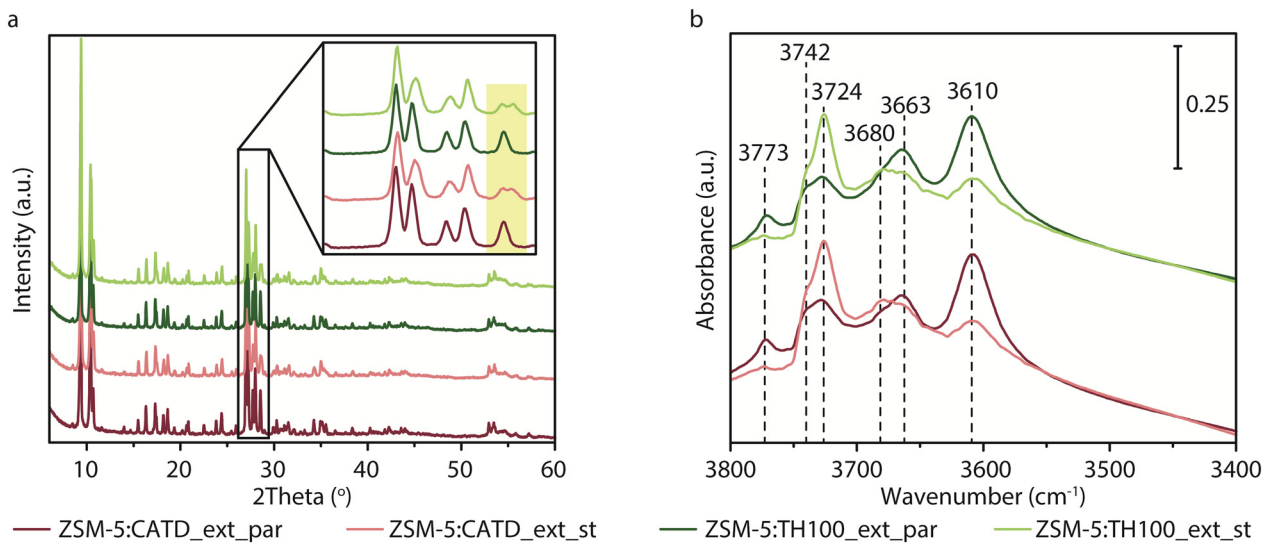

Fig. 6 Structural changes upon steaming. a) X-ray diffraction (XRD) patterns, b) Fourier-transform infrared (FT-IR) spectroscopy data taken under vacuum after drying at 550 °C for 2 h of the parent and 7 h steamed zeolite-based extrudates, using CATAPAL D (denoted as ZSM-5:CATD_ext_par, red, and ZSM-5:CATD_ext_st, light red, accordingly) and using PURAL TH100 (denoted as ZSM-5:TH100_ext_par, green, and ZSM-5:TH100_ext_st, light green, accordingly). Inset in (a) show the 2θ 26–29° region.

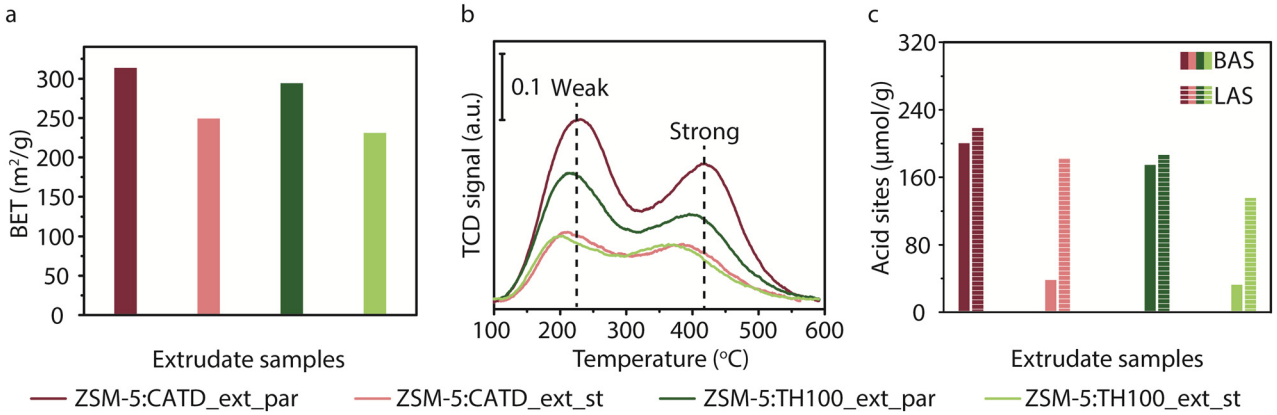

Fig. 7 Changes in the textural and acidic properties of the extrudate samples upon steaming. a) Brunauer–Emmett–Teller (BET) surface area calculated from Ar physisorption, b) ammonia temperature-programmed desorption (NH_3-TPD) analysis, c) Brønsted acid sites (BASs) and Lewis acid sites (LASs) as determined and calculated from Fourier-transform infrared (Py-FT-IR) spectroscopy after pyridine adsorption measured at 150 °C.

in the small zeolite pores. However, it still constitutes a valuable tool to calculate the number of BASs and LASs in the catalyst materials. After steaming, both samples seem to be similar in their overall acidity. The sample made using PURAL TH100 as a binder precursor material shows slightly weaker acid sites, as can be noted from the minor shift of the TPD curve to lower temperatures. Interestingly, Py-FT-IR spectroscopy measurements for the steamed samples revealed that they exhibited the same amount of BASs, while the sample with CATAPAL D as a binder precursor material after steaming exhibited higher amounts of LASs.

The aforementioned dissimilarity could be attributed to the physicochemical properties of the boehmite binder precursor. It can be expected that the CATAPAL D binder precursor material with a higher BET surface area (*i.e.*, 220 $m^2\ g^{-1}$), but also with a smaller crystallite size (*i.e.*, 7 nm) will have more accessible and/or "surface" aluminum atoms that will react more readily with water during the hydrothermal treatment compared to the PURAL TH100 binder precursor material with a lower BET surface area (*i.e.*, 150 $m^2\ g^{-1}$) and larger crystallite size (*i.e.*, 14 nm). The NH_3-TPD and Py-FT-IR spectroscopy proved the significant effect of the binder properties on the acidic properties of the zeolite-based shaped catalyst bodies. All in all, the porosity and the crystallite size of the binder material have a crucial role in the accessibility and the pore blockage phenomena and, thus, in combination with the hydrothermal treatment for the genesis of the required overall acidity as well as the appropriate BAS/LAS ratio.

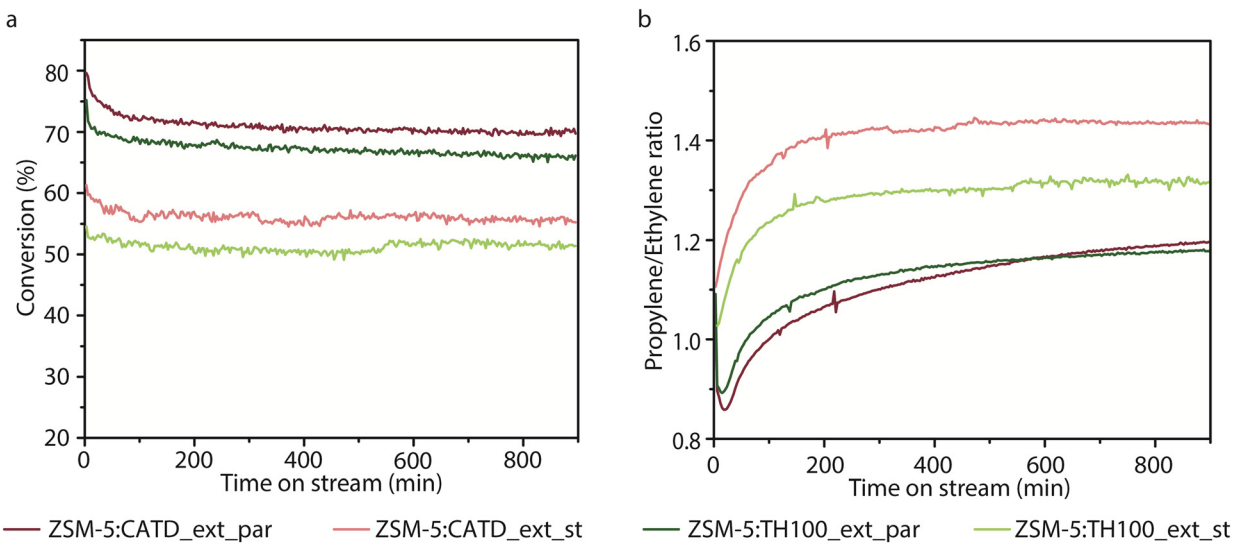

Fig. 8 Catalytic activity of shaped catalyst bodies in the methanol-to-hydrocarbon (MTH) reaction. (a) Conversion and (b) the ratio yields of ethylene *versus* propylene for the parent samples (denoted as ZSM-5:CATD_ext_par and ZSM-5:TH100_ext_par) and the steamed samples (denoted as ZSM-5:CATD_ext_st and ZSM-5:TH100_ext_st).

The catalyst extrudate samples, made using the two different boehmite binder precursor materials, were tested in the MTH reaction, before and after steaming, to evaluate the induced changes in the properties of the technical bodies. The parent extrudate samples, shown in Fig. 8a (ZSM-5:CATD_ext_par; dark red and ZSM-5:TH100_ext_par; dark green), show similar trends in terms of methanol conversion. The sample made using CATAPAL D as a binder precursor material shows a higher conversion (~71%), while the sample made using PURAL TH100 as a binder precursor material exhibits a lower conversion (~67%). This is due to the lower BET surface area as well as the lower acidity of the samples containing PURAL TH 100 as the MTH reaction is related to porosity/accessibility and acidity. After steaming, the samples containing CATAPAL D as a binder precursor material show an overall lower conversion (~56%), but still a higher one than the sample with PURAL TH 100 as a binder precursor material (~50%). The latter can be attributed to the higher BET surface area of the ZSM-5:CATD_ext_par sample as well as the higher amount of LASs present.

The two parent samples show similar propylene-to-ethylene ratios, as shown in Fig. 8b. This can be explained by the fact that the samples possess similar BAS/LAS ratios. However, hydrothermal treatment of the extrudate samples changed the propylene-to-ethylene ratio. It can be seen that the sample with CATAPAL D as a binder precursor material, after steaming, shows a higher propylene yield compared to the sample with PURAL TH 100 as a binder precursor material. Even though the two samples appeared to have the same total acidity, at least according to the NH_3-TPD measurements, they differ in the number of LASs with ZSM-5:CATD_ext_st having a higher amount of LASs, while they have the same number of BASs. These results align with a recent study from Yarulina *et al.*, where the interplay of LASs and BASs was key to optimal catalytic performance.

Experimental

Chemicals and materials

The following chemicals, gases, and materials were used: pyridine (C_5H_5N, Merck, EMSURE), methanol (Acros, HPLC grade, 99.99% pure), N_2 (Linde, 99.998%), He (Linde, >99%), and Ar (Linde, 99.998%).

Powder zeolite ZSM-5 was purchased from ACS Material (MR 38) with a silica/alumina ratio of 38. Shaped catalyst bodies were made from the zeolite ZSM-5 powder mixed with either the CATAPAL D or TH100 precursor as an alumina binder (provided by SASOL), methylcellulose (Sigma Aldrich, 4000 CP), acetic acid, and water using a mini-screw extruder (Caleva) through a 2 mm diameter die plate. The zeolite-to-binder ratio (total weight 20 g) is equal to 50 : 50 wt%. After drying overnight, the samples were calcined at 600 °C for 6 h (10 °C min^{-1}) under an air flow in a tubular oven.

Steaming treatments of the samples were performed in a quartz tubular oven at 500 °C for varying times (*i.e.*, 15, 30, 60, 10, 210, and 420 min) under a N_2 flow. The gas was passed first through a round-bottom flask containing water heated at a temperature of 100 °C to produce steam.

The zeolite ZSM-5 powder samples are denoted as ZSM-5_pow when ZSM-5_pow_par is used for the parent samples and ZSM-5_pow_st for the steamed samples. The extrudate samples are marked as ZSM-5:xx_ext, where xx can be either CATD or TH100, representing the CATAPAL D or TH100 alumina binder. Steamed extrudate samples are denoted as ZSM-5:xx_ext_st.

Materials characterization

X-ray diffraction (XRD) was measured on a Bruker D2 X-ray powder diffractometer with a Co Kα X-ray tube (λ = 1.7902 Å) as the source. Ammonia temperature-programmed desorption (NH_3-TPD) was measured on a Micromeritics AutoChemII 2920. Pyridine and CO adsorption followed by Fourier-transform infrared (FT-IR) spectroscopy was performed using a Bruker Vertex 70v spectrometer in the spectral range of 4000–1000 cm^{-1}. Experimental details of these measurements were described elsewhere.[26,39] N_2 physisorption measurements of the solids were performed using a Micromeritics TriStar 3000 instrument operating at −196 °C. Before completing the measurements, the samples were dried for 15 h at 300 °C under an N_2 flow.

Catalytic testing

The catalytic performance of the samples was tested in an *operando* UV-vis spectroscopy set-up, equipped to perform MTH reactions. ~69 mg of the samples were placed in a fixed-bed reactor using a weight hourly space velocity (WHSV) of 8 h^{-1} at 350 °C. Methanol and the reaction products were measured using an Interscience compact gas chromatograph (GC). The set-up is equipped with an AvaSpec 2048 L spectrometer *via* a high-temperature UV-vis optical fiber probe which enables recording of *operando* UV-vis diffuse reflectance spectroscopy (DRS) data. More details of the set-up can be found elsewhere.[26,48] The experimental conditions employed for the catalytic performance tests were chosen in order to be comparable with other previous studies on shaped catalyst bodies of our group and other research groups.[9,15,16] Catalytic tests were repeated 3 times to ensure reproducibility.

Conclusions

The influence of the hydrothermal treatment on the physicochemical properties and the methanol-to-hydrocarbon (MTH) performance of different alumina-bound zeolite-based catalyst extrudates was studied using a combination of *ex situ*, *in situ*, and *operando* characterization techniques. Zeolite powder and zeolite-based catalyst extrudates were compared before and after steaming. FT-IR spectroscopy on the extrudate samples confirmed that the extrusion process induced defects in the zeolite framework structure, while, after hydrothermal treatments, they presented extra –OH

species due to the presence of an alumina binder. FT-IR spectroscopy in combination with pyridine as a probe molecule proved that the alumina binder material offers resistance and protects the zeolite material from dealumination during hydrothermal treatments. Catalytic testing in the MTH reaction showed that the parent extrudate sample exhibited a higher stability and, upon steaming, a higher propylene yield. Tuning the physicochemical properties of the alumina binder, by using different alumina precursor materials (namely CATAPAL D and PURAL TH100, differing in their surface area and crystallite size), showed to influence the yield towards light olefins. Higher formation of conjugated poly-aromatic species for the parent and steamed extrudate samples than the zeolite powder sample was revealed using *operando* UV-vis diffuse reflectance spectroscopy (DRS) due to the nature and pore architecture of the shaped catalyst bodies.

Conflicts of interest

There are no conflicts to declare.

Acknowledgements

This research has received funding from the European Union's EU Framework Program for Research and Innovation Horizon 2020 under Grant Agreement No. 721385 (MSCA-ETN SOCRATES – **https://etn-socrates.eu/**). Remco Dalebout, Lennart Weber, and Miguel Rivera-Torrente, all three from Utrecht University (UU), are acknowledged for performing the Ar physisorption measurements.

Notes and references

1 K. Yang, D. Zhang, M. Zou, L. Yu and S. Huang, *ChemCatChem*, 2021, **13**, 1414–1423.
2 E. T. C. Vogt, G. T. Whiting, A. Dutta Chowdhury and B. M. Weckhuysen, *Adv. Catal.*, 2015, **58**, 143–314.
3 *Handbook of Heterogeneous Catalysis*, ed. G. Ertl, H. Knözinger, F. Schütch and J. Weitkamp, Wiley-VCH Verlag, Weinheim, 2008.
4 S. Mitchell, N. L. Michels and J. Pérez-Ramírez, *Chem. Soc. Rev.*, 2013, **42**, 6094–6112.
5 G. T. Whiting, S. H. Chung, D. Stosic, A. D. Chowdhury, L. I. Van Der Wal, D. Fu, J. Zecevic, A. Travert, K. Houben, M. Baldus and B. M. Weckhuysen, *ACS Catal.*, 2019, **9**, 4792–4803.
6 G. T. Whiting, F. Meirer, M. M. Mertens, A. J. Bons, B. M. Weiss, P. A. Stevens, E. De Smit and B. M. Weckhuysen, *ChemCatChem*, 2015, **7**, 1312–1321.
7 G. T. Whiting, A. D. Chowdhury, R. Oord, P. Paalanen and B. M. Weckhuysen, *Faraday Discuss.*, 2016, **188**, 369–386.
8 S. P. Verkleij, G. T. Whiting, D. Pieper, S. Parres Esclapez, S. Li, M. M. Mertens, M. Janssen, A. J. Bons, M. Burgers and B. M. Weckhuysen, *ChemCatChem*, 2019, **11**, 4788–4796.
9 N. L. Michels, S. Mitchell and J. Pérez-Ramírez, *ACS Catal.*, 2014, **4**, 2409–2417.
10 J. S. J. Hargreaves and A. L. Munnoch, *Catal. Sci. Technol.*, 2013, **3**, 1165–1171.
11 *Industrial Catalysis: Optimizing Catalysts and Processes*, ed. R. I. Wijngaarden, K. R. Westerterp, A. Kronberg and A. N. R. Bos, Wiley-VCH Verlag, Weinheim, 2008.
12 I. Yarulina, A. D. Chowdhury, F. Meirer, B. M. Weckhuysen and J. Gascon, *Nat. Catal.*, 2018, **1**, 398–411.
13 M. Stöcker, *Microporous Mesoporous Mater.*, 1999, **29**, 3–48.
14 P. Tian, Y. Wei, M. Ye and Z. Liu, *ACS Catal.*, 2015, **5**, 1922–1938.
15 G. T. Whiting, N. Nikolopoulos, I. Nikolopoulos, A. D. Chowdhury and B. M. Weckhuysen, *Nat. Chem.*, 2019, **11**, 23–31.
16 S. Zhang, Y. Gong, L. Zhang, Y. Liu, T. Dou, J. Xu and F. Deng, *Fuel Process. Technol.*, 2015, **129**, 130–138.
17 J. Freiding and B. Kraushaar-Czarnetzki, *Appl. Catal., A*, 2011, **391**, 254–260.
18 X. Di Chen, X. G. Li, H. Li, J. J. Han and W. De Xiao, *Chem. Eng. Sci.*, 2018, **192**, 1081–1090.
19 I. M. Dahl and S. Kolboe, *Catal. Lett.*, 1993, **20**, 329–336.
20 U. Olsbye, S. Svelle, M. Bjrgen, P. Beato, T. V. W. Janssens, F. Joensen, S. Bordiga and K. P. Lillerud, *Angew. Chem., Int. Ed.*, 2012, **51**, 5810–5831.
21 E. E. Kolesnikova, T. K. Obukhova, N. V. Kolesnichenko, G. N. Bondarenko, O. V. Arapova and S. N. Khadzhiev, *Pet. Chem.*, 2018, **58**, 863–868.
22 S. Zhang, B. Zhang, Z. Gao and Y. Han, *React. Kinet., Mech. Catal.*, 2010, **99**, 447–453.
23 S. Zhang, B. Zhang, Z. Gao and Y. Han, *Ind. Eng. Chem. Res.*, 2010, **49**, 2103–2106.
24 C. Chen, Q. Zhang, Z. Meng, C. Li and H. Shan, *Appl. Petrochem. Res.*, 2015, **5**, 277–284.
25 H. Khezri, A. Izadbakhsh and A. A. Izadpanah, *Fuel Process. Technol.*, 2020, **199**, 106253.
26 J. Goetze and B. M. Weckhuysen, *Catal. Sci. Technol.*, 2018, **8**, 1632–1644.
27 I. Yarulina, S. Bailleul, A. Pustovarenko, J. R. Martinez, K. De Wispelaere, J. Hajek, B. M. Weckhuysen, K. Houben, M. Baldus, V. Van Speybroeck, F. Kapteijn and J. Gascon, *ChemCatChem*, 2016, **8**, 3057–3063.
28 I. Yarulina, K. De Wispelaere, S. Bailleul, J. Goetze, M. Radersma, E. Abou-Hamad, I. Vollmer, M. Goesten, B. Mezari, E. J. M. Hensen, J. S. Martínez-Espín, M. Morten, S. Mitchell, J. Perez-Ramirez, U. Olsbye, B. M. Weckhuysen, V. Van Speybroeck, F. Kapteijn and J. Gascon, *Nat. Chem.*, 2018, **10**, 804–812.
29 M. Dusselier, M. A. Deimund, J. E. Schmidt and M. E. Davis, *ACS Catal.*, 2015, **5**, 6078–6085.
30 M. Rostamizadeh and F. Yaripour, *J. Taiwan Inst. Chem. Eng.*, 2017, **71**, 454–463.
31 Z. Li, J. Martínez-Triguero, J. Yu and A. Corma, *J. Catal.*, 2015, **329**, 379–388.
32 K. Y. Lee, H. K. Lee and S. K. Ihm, *Top. Catal.*, 2010, **53**, 247–253.
33 J. Holzinger, P. Beato, L. F. Lundegaard and J. Skibsted, *J. Phys. Chem. C*, 2018, **122**, 15595–15613.

34 J. N. Louwen, L. Van Eijck, C. Vogt and E. T. C. Vogt, *Chem. Mater.*, 2020, **32**, 9390–9403.
35 N. Nikolopoulos, R. G. Geitenbeek, G. T. Whiting and B. M. Weckhuysen, *J. Catal.*, 2021, **396**, 136–147.
36 H. W. Huang, H. Zhu, S. H. Zhang, Q. Zhang and C. Y. Li, *J. Fuel Chem. Technol.*, 2019, **47**, 74–83.
37 Y. Wang, Y. Chang, M. Liu, A. Zhang and X. Guo, *Molecules*, 2019, **24**, 3462.
38 A. A. Gabrienko, I. G. Danilova, S. S. Arzumanov, D. Freude and A. G. Stepanov, *ChemCatChem*, 2020, **12**, 478–487.
39 E. A. Uslamin, B. Luna-Murillo, N. Kosinov, P. C. A. Bruijnincx, E. A. Pidko, B. M. Weckhuysen and E. J. M. Hensen, *Chem. Eng. Sci.*, 2019, **198**, 305–316.
40 J. Li, D. Han, Z. Zi, T. He, G. Liu, Z. Wang, J. Wu and J. Wu, *Fuel*, 2022, **313**, 122643.
41 K. Chen, X. Wu, J. Zhao, H. Zhao, A. Li, Q. Zhang, T. Xia, P. Liu, B. Meng, W. Song, X. Zhu, H. Liu, X. Gao, C. Xu and B. Shen, *J. Catal.*, 2022, **413**, 735–750.
42 C. Hammond, N. Dimitratos, J. A. Lopez-sanchez, R. L. Jenkins, G. Whiting, S. A. Kondrat, M. Hasbi, M. M. Forde, A. Thetford, H. Hagen, E. E. Stangland, J. M. Moulijn, S. H. Taylor, D. J. Willock and G. J. Hutchings, *ACS Catal.*, 2013, **3**, 1835–1844.
43 K. Sadowska, K. Góra-Marek, M. Drozdek, P. Kuśtrowski, J. Datka, J. Martinez Triguero and F. Rey, *Microporous Mesoporous Mater.*, 2013, **168**, 195–205.
44 M. Digne, P. Sautet, P. Raybaud, P. Euzen and H. Toulhoat, *J. Catal.*, 2002, **211**, 1–5.
45 H. Knözinger and P. Ratnasamy, *Catal. Rev.: Sci. Eng.*, 1978, **17**, 31–70.
46 L. H. Ong, M. Dömök, R. Olindo, A. C. Van Veen and J. A. Lercher, *Microporous Mesoporous Mater.*, 2012, **164**, 9–20.
47 Z. Yu, S. Li, Q. Wang, A. Zheng, X. Jun, L. Chen and F. Deng, *J. Phys. Chem. C*, 2011, **115**, 22320–22327.
48 J. Goetze, F. Meirer, I. Yarulina, J. Gascon, F. Kapteijn, J. Ruiz-Martínez and B. M. Weckhuysen, *ACS Catal.*, 2017, **7**, 4033–4046.
49 M. J. Wulfers and F. C. Jentoft, *ACS Catal.*, 2014, **4**, 3521–3532.
50 J. Goetze, I. Yarulina, J. Gascon, F. Kapteijn and B. M. Weckhuysen, *ACS Catal.*, 2018, **8**, 2060–2070.
51 D. Fu, O. van der Heijden, K. Stanciakova, J. E. Schmidt and B. M. Weckhuysen, *Angew. Chem., Int. Ed.*, 2020, **59**, 15502–15506.
52 J. Valecillos, Z. Tabernilla, E. Epelde, E. Sastre, A. T. Aguayo and P. Castaño, *Ind. Eng. Chem. Res.*, 2020, **59**, 13892–13905.
53 J. Valecillos, H. Vicente, A. G. Gayubo, A. T. Aguayo and P. Castaño, *J. Catal.*, 2022, **408**, 115–127.
54 J. Valecillos, E. Epelde, J. Albo, A. T. Aguayo, J. Bilbao and P. Castaño, *Catal. Today*, 2020, **348**, 243–256.